JOURNAL OF GEOPHYSICAL RESEARCH, VOL. 102, NO. A3, PAGES 4751-4764, MARCH 1, 1997

Plasma wave characteristics of the Jovian magnetopause boundary layer: Relationship to the Jovian aurora?

Bruce T. Tsurutani,[1] John K. Arballo,[1] Bruce E. Goldstein,[1] Christian M. Ho,[1] Gurbax S. Lakhina,[1] Edward J. Smith,[1] Nicole Cornilleau-Wehrlin,[2] Renée Prangé,[3] Naiguo Lin,[4] Paul Kellogg,[4] John L. Phillips,[5] Andre Balogh,[6] Norbert Krupp,[7] and Mark Kane [8]

Abstract. The Jovian magnetopause boundary layer (BL) plasma wave spectra from 10^{-3} to 10^{2} Hz have been measured for the first time. For one intense event the magnetic (B') and electric (E') spectra were $2 \times 10^{-4} f^{-2.4}$ nT^2/Hz and $4 \times 10^{-9} f^{-2.4}$ V^2/m^2 Hz, respectively. Although no measurable wave amplitudes were detected above the electron gyrofrequency, ~140 Hz, this finding may be due to the low signal strength characteristic of this region. The B'/E' ratio is relatively frequency independent. It is possible that waves are obliquely propagating whistler mode waves. The B' and E' spectra are broadband with no obvious spectral peaks. The waves are sufficiently intense to cause cross-field diffusion of magnetosheath plasma to create the BL itself. A Jovian BL thickness of 10,700 km is predicted, which is consistent with past in situ measurements. The Jovian boundary layer wave properties are quite similar to the BL waves at Earth (however, the Jovian waves are orders of magnitude less intense). It appears that the solar wind/magnetosphere dynamos at the two planets are similar enough to be consistent with a common wave generation mechanism. The predicted ionospheric latitudinal width of the BL of ~100-200 km is quite similar to the Jovian auroral high-latitude ring measured by Hubble. The location of the BL at and inside the foot point of the last closed field line may place the boundary layer and the aurora on approximately the same magnetic field lines. The Jovian BL waves are sufficiently intense to cause strong pitch angle diffusion for <5-keV electrons and 1-keV to 1-MeV protons. The estimated energy precipitation rate from this interaction <1 erg cm^{-2} s^{-1}, sufficient for a weak high-latitude auroral ring. This intensity is 2 to 3 orders of magnitude too low to cause the main aurora ring, however. If it is found that this main aurora maps into the boundary layer, then other mechanisms such as (ionospheric) double layers must be responsible for the particle energization and precipitation.

Introduction

Plasma waves present in the Earth's magnetopause boundary layer (BL) are important for several fundamental geophysical processes. First, they are products of plasma instabilities associated with strong particle anisotropies and/or plasma and field gradients, or they are resonantly amplified magnetosheath waves. Second, through resonant interactions with charged particles, they are important for momentum and energy transfer from the solar wind to the magnetosphere/ ionosphere. Concerning the first topic, that of a wave source, several instabilities/mechanisms have been discussed in the literature [*Kennel and Petschek*, 1966; *D'Angelo*, 1973; *Ashour-Abdalla and Thorne*, 1977; *Swift*, 1977; *Huba et al.*, 1978; *LaBelle and Treumann*, 1988; *Rezeau et al.*, 1989; *Belmont et al.*, 1995]. However, at this time there has been little agreement as to the specific mechanism(s). The broadband nature of the waves with a lack of accompanying peaks [*Gurnett et al.*, 1979; *Anderson et al.*, 1982; *Tsurutani et al.*, 1989] has made such identification extremely difficult. The relative constancy of the power law spectra over all local times [*Tsurutani et al.*, 1989] is another observation that should be taken into account. A recent model involving the current convection instability evolving to a strongly turbulent state [*Drake et al.*, 1994] seems promising. However, only the electrostatic case has been studied thus far.

The magnetopause boundary layer waves have been speculated to be important for two different types of particle transport. First, the waves have been shown to be capable of diffusing solar

[1]Jet Propulsion Laboratory, California Institute of Technology, Pasadena.
[2]Centre d'Etude des Environnements Terrestre et Planétaires/Université Versailles-Saint-Quentin, Vélizy, France.
[3]Institute d'Astrophysique Spatiale, University of Paris XI, Orsay, France.
[4]University of Minnesota, School of Physics and Astronomy, Minneapolis.
[5]Los Alamos National Laboratory, Los Alamos, New Mexico.
[6]Blackette Laboratory, Imperial College of Science and Technology, London, England.
[7]Max-Planck-Institut für Aeronomie, Katlenburg-Lindau, Germany.
[8]Applied Physics Laboratory, Johns Hopkins University, Laurel, Maryland.

Paper number 96JA02785.
0148-0227/97/96JA-02785$09.00

wind/magnetosheath plasma onto closed (magnetospheric) field lines at a rate rapid enough to form the magnetopause boundary layer itself *[Tsurutani and Thorne*, 1982; *Gendrin*, 1983; *Thorne and Tsurutani*, 1991]. This action can be thought of as a specific "viscous interaction" mechanism [*Axford and Hines*, 1961; *Cole*, 1961; *Tsurutani and Gonzalez*, 1995], in which the solar wind flow energy is transferred to the magnetosphere. Second, rapid pitch angle scattering of energetic particles via cyclotron resonant interactions with the waves can provide significant particle losses to the ionosphere creating the dayside aurora at Earth [*Tsurutani et al.*, 1981], a phenomenon that is ever present and is independent of substorms.

Auroral emissions are also observed in the polar atmosphere of Jupiter. Most of the mechanisms initially proposed for the Jovian aurora [*Thorne and Tsurutani*, 1979; *Thorne*, 1981, 1983; *Thorne and Moses*, 1983; *Gehrels and Stone*, 1983; *Herbert et al.*, 1987; *Prangé and Elkhamsi*, 1990] have depended on enhanced wave-particle interactions with electrons, protons, and/or heavy ions, in and near the Io torus, on magnetic shells crossing the equator between ≅ 6 and 12.

The recent access to imaging in the UV wavelength range with the Hubble Space Telescope (HST) has changed our view significantly and have shown that the Jovian aurora has a complex morphology with a number of different structures [*Gérard et al.*, 1993] presumably due to different auroral precipitation processes. Permanent features include an emission fixed in magnetic longitude at the footprint of field lines connected to the Io torus, where intense ion cyclotron waves have simultaneously been detected [*Rezeau et al.*, 1996], and to a series of higher-latitude features, including polar cap emissions and a bright narrow oval surrounding each pole, to be associated with phenomena occurring on more distant magnetic field lines [Prangé et al., 1996a,b].

A plasma boundary layer has been identified inside the Jovian magnetopause[*Lanzerotti et al.*, 1979; *Sonnerup et al.*, 1981; *Scudder et al.*, 1981]. Most recently, *Phillips et al.* [1993] have identified 14 crossings, using the Ulysses Jupiter flyby data. *Tsurutani et al.* [1993] reported the detection of electromagnetic waves at the proton cyclotron frequency at a limited number of these crossings. They have also determined the cross-field diffusion rate, using measured wave amplitudes, and have shown them to be sufficient to form the Jovian boundary layer. In fact, the calculated thickness is quite similar to that during Pioneer 10 and 11 crossings when triple crossings were used to experimentally determine the spatial thickness [*Sonnerup et al.*, 1981].

Galvin et al. [1993], using the Ulysses solar wind ion composition spectrometer observations, have identified ion species of both Jovian magnetospheric origin (O^+, O^{2+}, S^{2+}, S^{3+}) and sheath origin (He^{2+}, high charge states of CNO) within the BL. Ions of magnetospheric origin are also found within the Jovian magnetosheath. These observations clearly indicate that charged particle transport across the magnetopause boundary is occurring in both directions.

The purpose of this paper is twofold. First, we will examine all 14 of the *Phillips et al.* [1993] Jovian boundary layer crossings to characterize for the first time the E' and B' wave spectra within this region of space. For the magnetic field we will combine the dc magnetometer and ac search coil data sets to get extended spectra from dc to ELF frequencies. We will also examine the electric field spectra. These E' and B' spectra will be compared and contrasted with those at the Earth's boundary layer to determine the commonality/lack of commonality of the wave properties at the two different planetary magnetospheres. This important information will give constraints for any (common) model of wave generation. The ratio of E' and B' amplitudes will be used to attempt to determine how much of the spectrum is due to electromagnetic waves and how much is electrostatic (see discussion *by Gurnett et al.*, [1979]).

Second, the width of the BL at ionospheric heights will be calculated and compared with the high-latitude auroral ring. Using the measured BL wave power and measured energetic particle flux, we will calculate and discuss the pitch angle diffusion rates and particle losses into the Jovian ionosphere in light of recent Hubble observations of the Jovian aurora [*Gérard et al.*, 1994; *Rego et al.*, 1994, 1996; *Clarke et al.*, 1995; *Prangé et al.*, 1996a,b].

Method of Analyses

The Ulysses magnetometer experiment is described by *Balogh et al.* [1992]. The vector helium sensor portion of this instrument has a temporal resolution of 1 vector s^{-1}, the resolution used in this study. The Ulysses radio and plasma wave (URAP) instrument is described by *Stone et al.* [1992]. There are 10 low-band and 12 high-band channels. The low-band channels extend from 0.22 to 5.3 Hz, and the high-band channels extend from 9.3 to 448 Hz. For the high-band channels, electric and magnetic fields are measured perpendicular to the spin axis, called E_x and B_y. Data from the URAP and magnetometer instruments have been merged to form a continuous spectrum in B'. The URAP E' data are used for the electric part of the spectrum.

The URAP wave background levels are determined for each frequency channel by averaging a number of lowest values of the signals during selected "quiet periods" when there was little wave activity. These averages of lowest values are taken as the instrument background noise. Also, the background levels are determined separately for two different scan modes of another instrument (plasma frequency receiver), which produce different noise levels in the waveform analyzer. There are therefore two different background levels for the events analyzed.

The heliosphere instrument for spectra composition and anisotropy at low energy (HI-SCALE) consists of five detector apertures in two separate telescope assemblies, which form different angles with the spacecraft spin axis [*Lanzerotti et al.*, 1992]. HI-SCALE can measure electrons with energies between 40 and 300 keV in four different channels and ions (Z31) with energies between 50 and 5000 keV (assuming protons) in eight different channels.

The five detectors are identified as LEMS30, LEFS60, LEMS120, LEFS150, and CA60. The numbers in the names indicate the orientation of the telescopes' central axes relative to the spin axis of the spacecraft. During each 12-s rotation the measured ions and electrons are sampled into four (LEMS30, LEFS150) and eight sectors (LEMS120, LEFS60, CA60), respectively. The HI-SCALE instrument provides measurements from 32 various directions in space with a high time resolution of 12 or 24 s. More detailed information about the instrument can be found in the paper by *Lanzerotti et al.*[1992].

The Jovian boundary layer waves are analyzed for the periods indicated by *Bame et al.*[1992a] and *Phillips et al.* [1993]. The density, temperature, and distribution function signatures are the most reliable ones for the identification of the start and stop times for the boundary layer (at Jupiter). All 14 intervals of the inbound (~1100 local time) and outbound passes (~1800 local time) have been studied.

Results

Waves

Table 1, modified from *Phillips et al.* [1993], gives the 14 time intervals for the Ulysses Jovian BL crossings. These intervals

Table 1. The 14 BL crossings identified by *Phillips et al.* [1993]

			Entry			Exit		
Event	Transition	Boundary	Date	Day of Year	Time, UT	Date	Day of Year	Time, UT
1	Msh-BL-Msh	MP1	Feb. 2, 1992	033	2130	Feb. 2, 1992	033	2308
		MP2	Feb. 2, 1992	033	2222	Feb. 2, 1992	033	2308
2	Msp-BL-Msh	MP	Feb. 3, 1992	034	1655	Feb. 3, 1992	034	1720
3	Msh-BL-Msh	MP	Feb. 3, 1992	034	1945	Feb. 4, 1992	035	0025
4	Msh-BL-Msh	MP	Feb. 4, 1992	035	0100	Feb. 4, 1992	035	0125
5	Msh-BL-Msp	MP	Feb. 4, 1992	035	0250	Feb. 4, 1992	035	0400
6	Msp-BL-Msp		Feb. 12, 1992	043	0024	Feb. 12, 1992	043	0100
7	Msp-BL-Msp		Feb. 12, 1992	043	1058	Feb. 12, 1992	043	1226
8	Msp-BL-Msh	MP	Feb. 12, 1992	043	1337	Feb. 12, 1992	043	1357
9	Msh-BL-Msp	MP	Feb. 12, 1992	043	1700	Feb. 12, 1992	043	1740
10	Msp-BL-Msh	MP	Feb. 12, 1992	043	1820	Feb. 12, 1992	043	1910
11	Msh-BL-Msp	MP	Feb. 14, 1992	045	0933	Feb. 14, 1992	045	1030
12	Msp-BL-Msp		Feb. 14, 1992	045	1400	Feb. 14, 1992	045	1600
13	Msp-BL-Msp		Feb. 14, 1992	045	1815	Feb. 14, 1992	045	1825
14	Msp-BL-Msh	MP	Feb. 14, 1992	045	2045	Feb. 14, 1992	045	2140

Magnetosheath (Msh), boundary layer (BL), and magnetosphere (Msp), with identification of the boundary crossed, bow shock (BS) or magnetopause (MP). MP1 - based on magnetic field observations. MP2 - based on plasma observations. There are five crossings on the Ulysses inbound pass, days 33-35, 1992, and nine crossings on the outbound pass, days 43-45, 1992. The events have been numbered in chronological order for ease of description.

were identified by using the plasma density and velocity characteristics alone. For the BL intervals the plasma parameters (including temperature) were intermediate between those of the magnetosheath and magnetosphere. From left to right the columns are the event number, the type of transition, the entry time, and the exit time. There are five crossings on the inbound pass (days 33-35, 1992) and nine crossings on the outbound pass (days 43-45, 1992). Throughout the paper we will use the event numbers (listed chronologically), rather than the dates, to save space.

Figure 1 gives an overview of the low-frequency E' and B' waves for all 14 BL events. From top to bottom are the E' spin plane average 9.3-, 14-, 19- and 28-Hz channel wave intensities; the B' spin plane average wave intensities for the same frequency channels; the B' 1-min and 10-min variances (taken from the dc magnetometer); and the spacecraft location relative to the planet. The shaded intervals are the Phillips et al. designated BL intervals. Bow shock crossings are indicated by vertical dashed lines. Magnetosheath or BL intervals are given by solid horizontal bars in the top panel.

Several features are readily apparent from Figure 1. Above background wave intensities are sometimes present in frequency channels ranging from 9.3 Hz (displayed) up to the electron cyclotron frequency. When present, the enhanced signals are most noticeable in the lowest frequency channels shown. Although there are similar large wave amplitudes in the magnetosheath region (nonshaded intervals indicated by horizontal bars), the magnetosheath signals are generally less intense than those in the boundary layer. This situation is similar to that for the Earth's BL/magnetosheath waves [*Gurnett et al.*, 1979; *Anderson et al.*, 1982].

The B' wave intensities have a different signature. Typically, the magnetosheath and boundary layer intervals are quiet (near instrument background) in the ELF/VLF frequency range, especially for the inbound pass. However, on the outbound pass for days 43 and 44, and also the beginning of day 45, the BL and magnetosheath ELF wave intensities were noticeably more intense. The waves were most prominent in the lowest frequency channels (see the 9.3- and 14-Hz channels).

The 1-min and 10-min variances derived from the 1-s dc magnetometer data were also low on the inbound pass, but considerably more intense on the outbound pass. The variance values were highest on the outbound pass on day 43. The magnetosheath values on this day were high as well.

The interplanetary plasma conditions were considerably different on the inbound pass from those on the outbound pass. On the inbound pass the velocity and density were 510 km/s and 0.07 cm^{-3}, and on the outbound pass they were 395 km/s and 0.3 cm^{-3} (J. L. Phillips, private communication, 1995). Because of the unusually low ram pressure during the inbound pass the magnetosphere was greatly extended at encounter [*Smith and Wenzel,* 1993]. The solar wind ram pressure was more normal during the outbound pass. From the wave measurements it is clear that the ram pressure has a direct effect on BL wave intensities (in comparison, only the magnetosheath B_z has an effect on wave intensity at Earth [*Tsurutani et al.*, 1989]).

Figure 2a illustrates the power spectra for the magnetometer data for all 14 BL intervals. Each spectrum has been fitted to a power law and is shown in Figure 2b. All of the spectra are similar in shape, varying primarily in intensity. The most intense intervals (events 8, 9, and 10) are more than 1 order of magnitude greater in intensity than the average. These latter events are called out in Figure 2b.

Figure 3 illustrates the URAP B' ELF wave power spectra for 14 BL intervals. Almost all events are at or near instrument threshold levels, except near a narrow frequency range of 1-10 Hz. The two different instrument background levels noted at 20-400 Hz are due to the instrument mode selection (some instrument self-interference).

Since the day 43 events are the most significant in terms of wave intensity, we will focus our attention on these events, particularly on events 9 and 10. The E' and B' spectra for events 9 and 10 (day 43) are shown in Figures 4 and 5, respectively. The electric wave spectra are given in the left-hand panels. The instrument background is also shown. The E' spectra have a $1.2 \times 10^{-9} f^{-2.3} V^2/m^2$ Hz fit and a $4.1 \times 10^{-9} f^{-2.4} V^2/m^2$ Hz fit for the two intervals. The spectra are broadbanded with no obvious peaks within the frequency range examined. The event 10 spectrum is

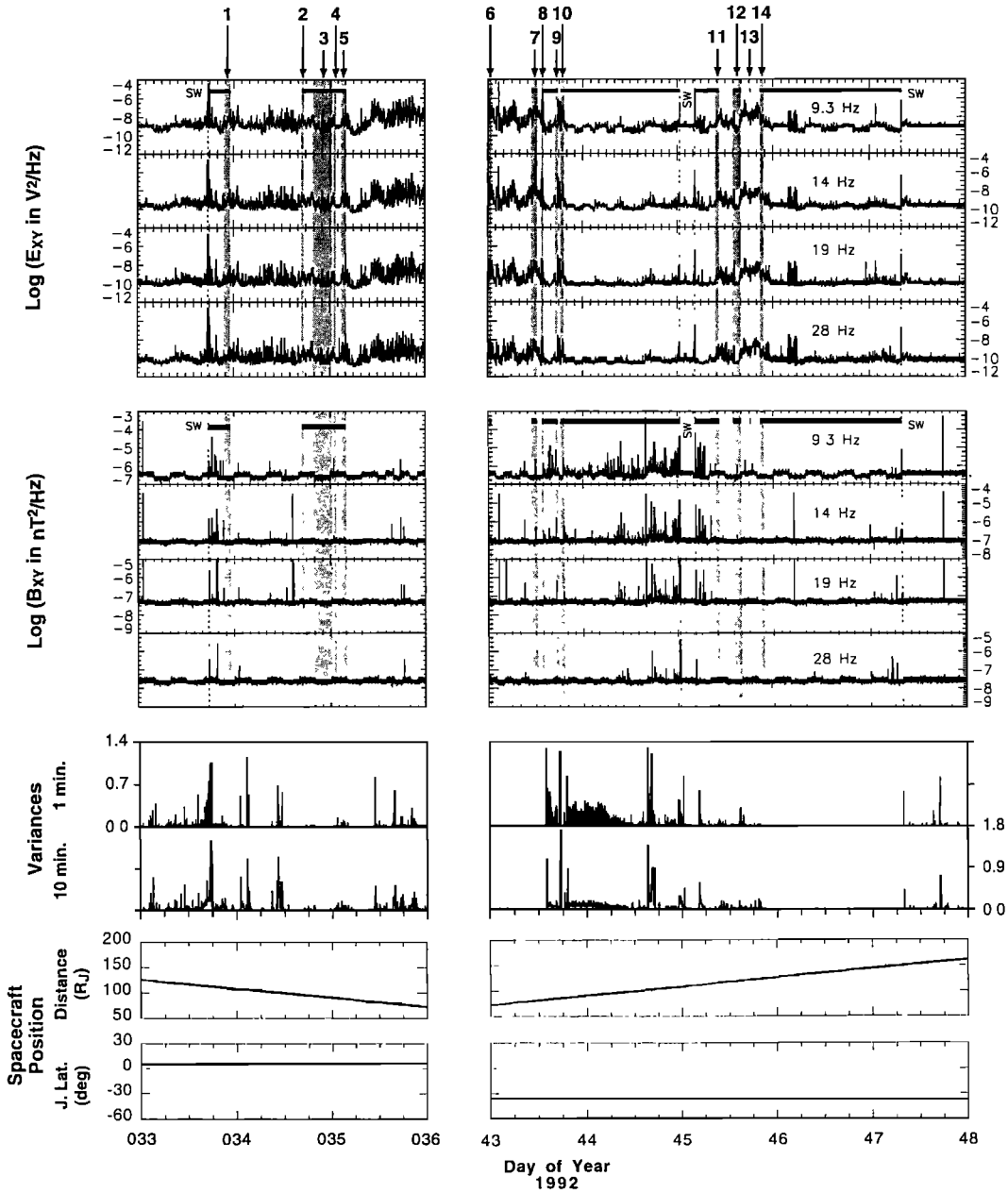

Figure 1. An overview of the low-frequency E' and B' wave amplitudes for all 14 BL events. The inbound pass is shown on the left and the outbound on the right. The top four panels contain the spin plane average E', the next four contain the spin plane average B', the next two contain the dc magnetometer variances, and the bottom two show spacecraft location. The BL events are shaded and numbered. Bow shock crossings are indicated by vertical dashed lines, and magnetosheath/BL intervals are indicated by horizontal bars. The BL wave intensities were high on the outbound pass when the solar wind ram pressure was more normal (the ram pressure was abnormally low on the inbound pass).

higher across the whole frequency range than the event 9 spectrum. Event 10 also has a spectral shape that is independent from that of the background curve, indicating that the natural wave power is dominating the spectrum.

The ELF B' spectra for events 9 and 10 are shown in the right-hand panels of Figures 4 and 5. The signals are above instrument background in the range 1 Hz to 10^2 Hz. The power law fits to these two events are $1.8 \times 10^{-4} f^{-2.2}$ and $3.5 \times 10^{-4} f^{-2.5}$ nT²/Hz, respectively. The wave intensities were greatest at the very beginning of the two events. One minute averages of this portion of the BL crossings were generated and are indicated as B_{max} curves.

The magnetic spectra for events 9 and 10 at lower frequencies (2×10^{-3} to 5×10^{-1} Hz) were given in Figure 2. They were obtained from the vector helium (dc) magnetometer which has an instrument noise level independent of frequency. This level is indicated in Figure 2a. Note that the shapes of the two power spectra (see Figure 2a) are remarkably similar to those determined for the higher-frequency URAP data.

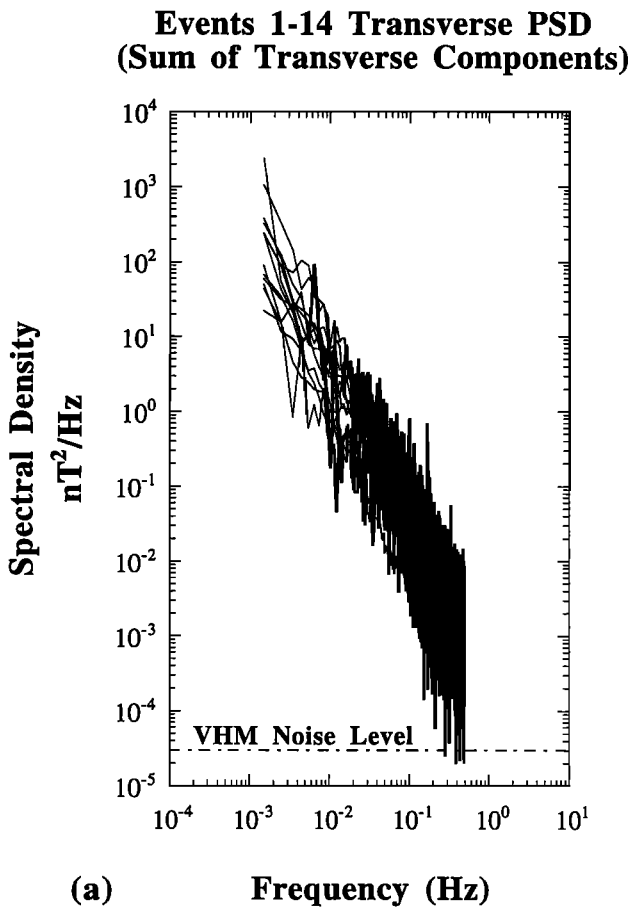

The spectra can be fitted together by extrapolating the dc magnetometer power spectra to the higher ELF frequencies of the URAP experiment. This process is shown by dashed lines in Figure 6. Event 9 is shown on the left, and event 10 is shown on the right. Thus the two curves join smoothly together at ~1.0 Hz as expected (the sensitivity of dc magnetometers and search coils becomes comparable at ~1 Hz). The part of the search coil curve for frequencies below this level is purely instrument noise.

If we make a fit to the overall combined magnetic spectra, we get $2.4 \times 10^{-4}\ f^{-2.2}$ nT²/Hz and $1.8 \times 10^{-4}\ f^{-2.4}$ nT²/Hz, respectively. It is interesting to note that the frequency dependencies on the power spectra for E' and B' are similar. We will comment on this feature somewhat later.

To determine whether the broadband BL waves are purely electromagnetic or instead are a combination of both electromagnetic and electrostatic waves, we calculate the B'/E' ratio as taken from event 10, an interval of day 43 when the wave amplitudes were the highest. The results are given in Figure 7. At 1 Hz, B'/E' ~200. The ratio decreases with increasing frequency but then increases from 10^1 Hz to above 10^2 Hz. Overall, the ratio has a relatively constant value near ~100.

For purely electromagnetic, parallel propagating waves, $B'/E' = n = c/V_{ph}$, where n is the index of refraction, c is the velocity of light, and V_{ph} is the phase velocity of the wave. For

Figure 2. (a) Power spectra from the dc magnetometer for all 14 BL intervals. (b) Power law fits to the spectra. All spectra are similar in shape, varying primarily in intensity. The most intense intervals are events 8, 9, and 10.

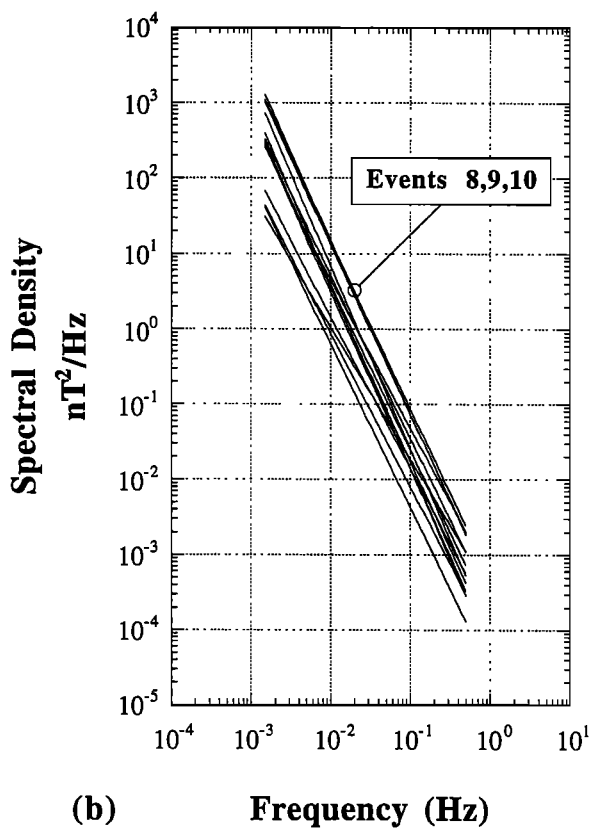

Event	I
1	$(9.8 \times 10^{-5}) f^{-2.4}$
2	$(7.2 \times 10^{-5}) f^{-2.0}$
3	$(2.9 \times 10^{-5}) f^{-2.2}$
4	$(6.6 \times 10^{-5}) f^{-2.3}$
5	$(5.4 \times 10^{-5}) f^{-2.4}$
6	$(8.6 \times 10^{-5}) f^{-2.3}$
7	$(1.6 \times 10^{-4}) f^{-2.2}$
8	$(3.7 \times 10^{-4}) f^{-2.3}$
9	$(5.1 \times 10^{-4}) f^{-2.2}$
10	$(4.1 \times 10^{-4}) f^{-2.3}$
11	$(2.4 \times 10^{-4}) f^{-2.2}$
12	$(1.4 \times 10^{-4}) f^{-2.0}$
13	$(5.2 \times 10^{-4}) f^{-2.0}$
14	$(3.3 \times 10^{-4}) f^{-1.8}$

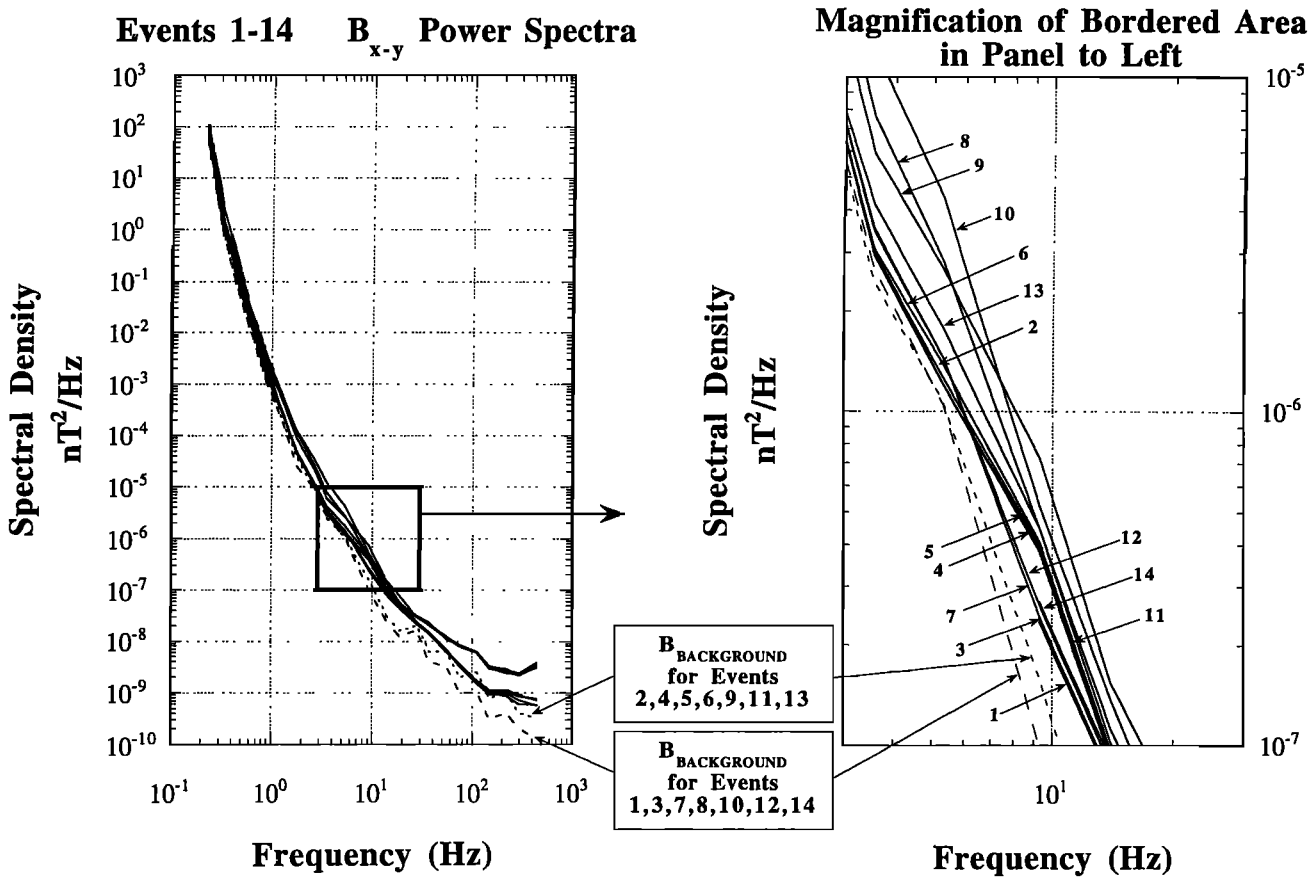

Figure 3. The spectra for the URAP *B'* ELF waves. Note that almost all events are at or near instrument threshhold, except for a narrow region near 1-10 Hz.

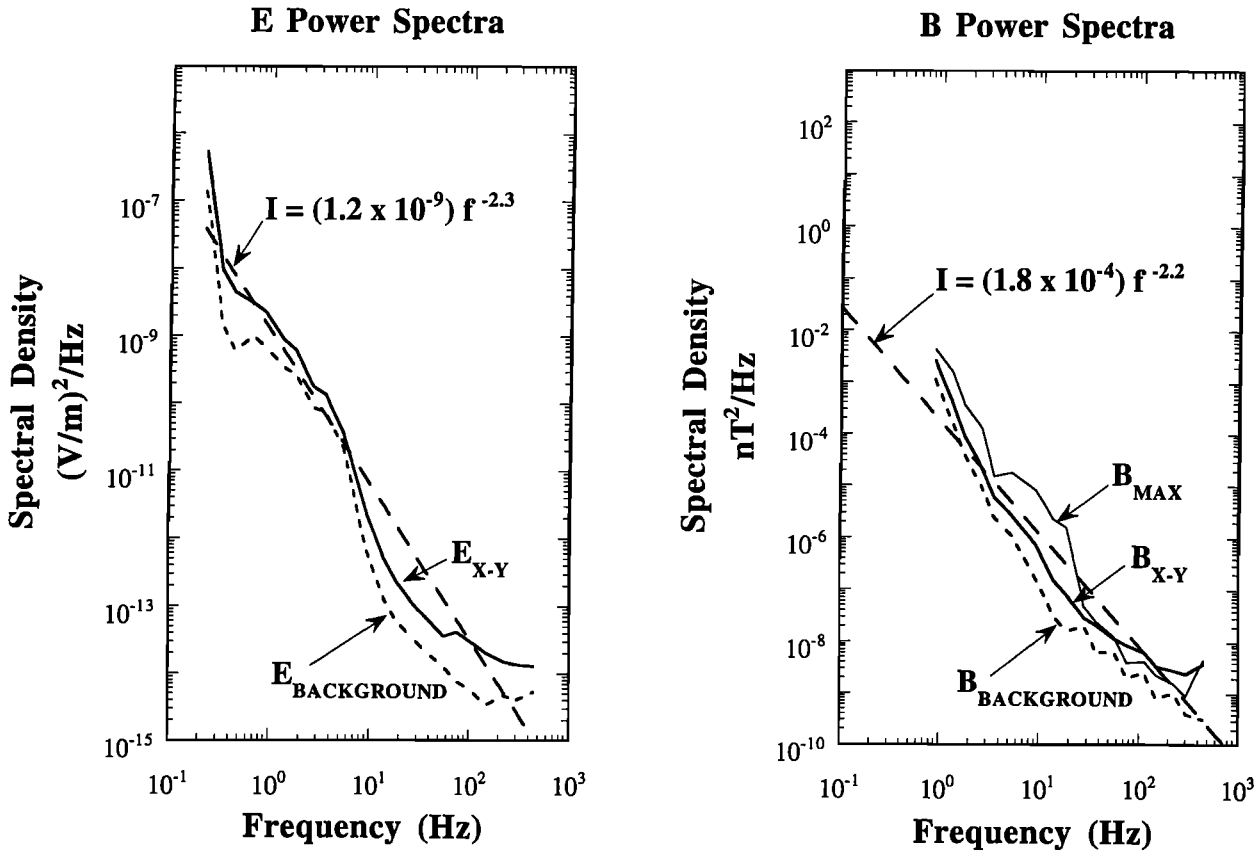

Figure 4. The electric (left) and magnetic (right) wave spectra for event 9. The spectra are broadband with no obvious peaks.

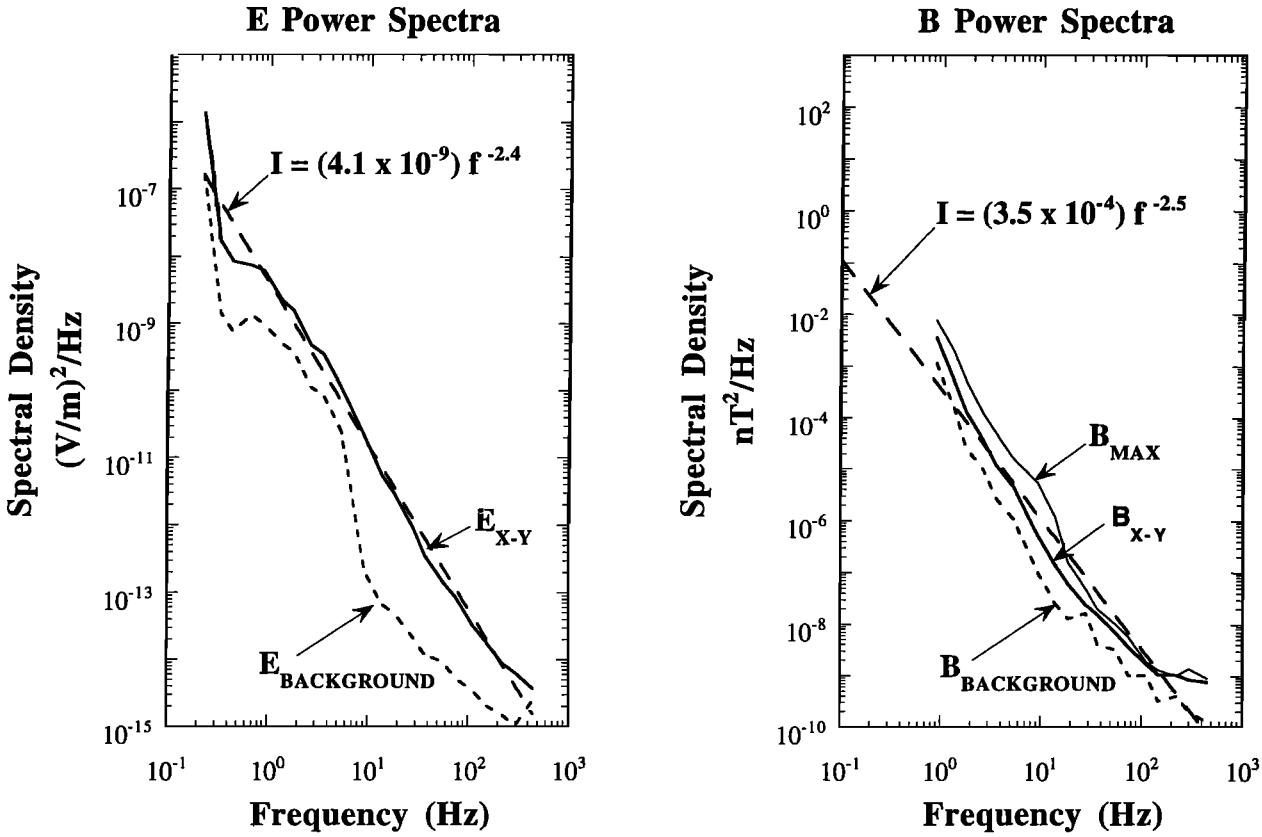

Figure 5. The same as Figure 4 but for event 10. The wave power in both E' and B' are highest in this event.

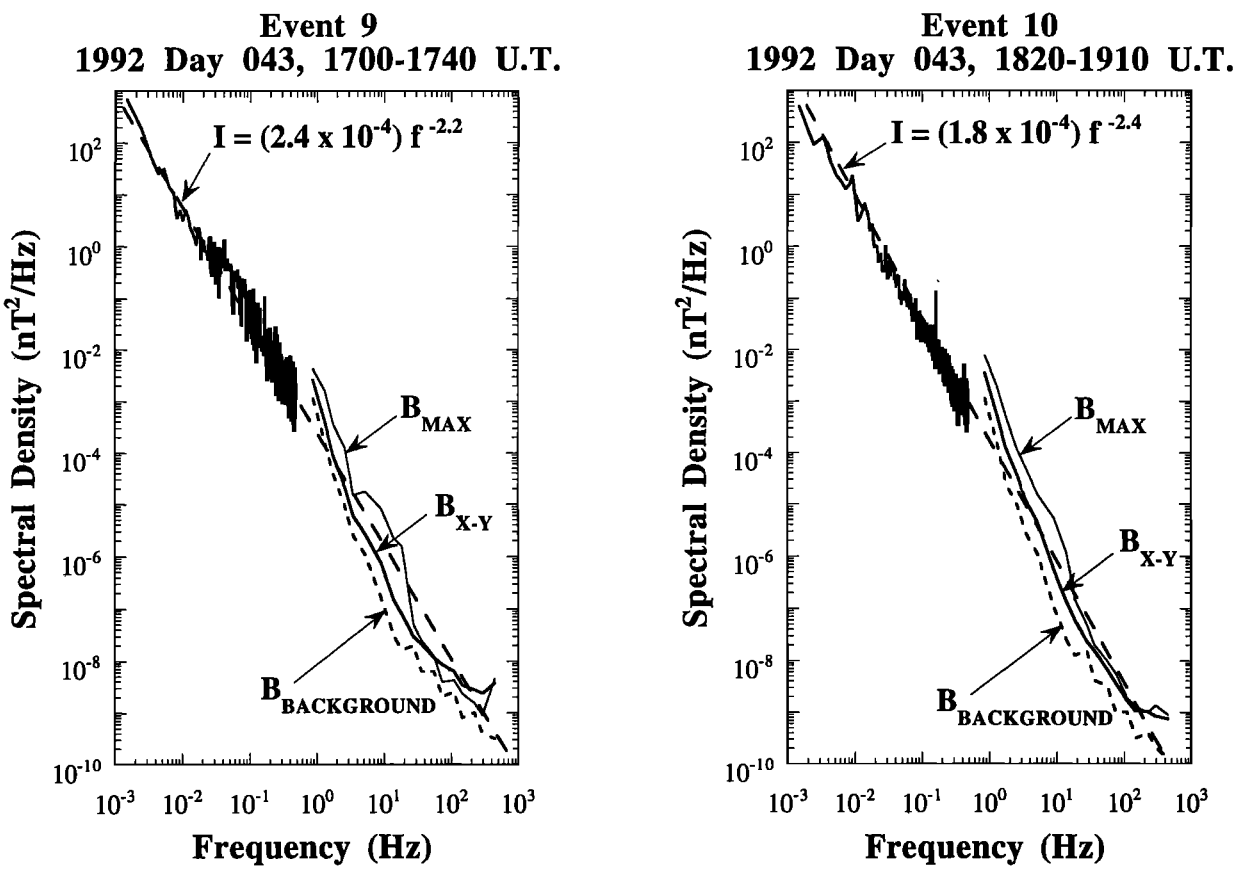

Figure 6. Combined MAG and URAP magnetic spectra for events 9 and 10. The dc power spectra are extrapolated to higher frequencies by dashed lines. The dc and ac magnetometer spectra join smoothly at ~1 Hz, as theoretically expected.

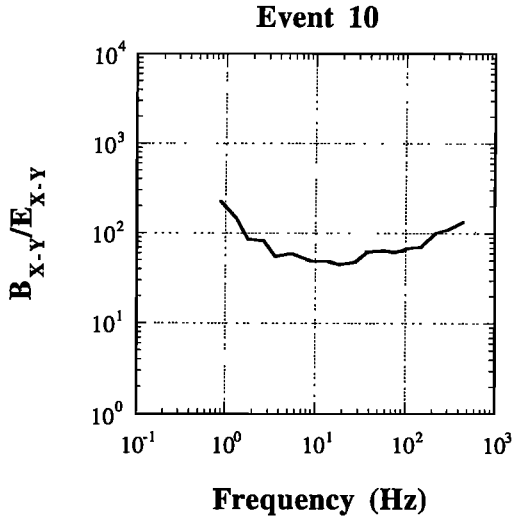

B_{X-Y}/E_{X-Y} at selected frequencies

Frequency (Hz)	B_{X-Y}/E_{X-Y}
1	2.0×10^2
3	7.0×10^1
10	4.9×10^1
30	5.1×10^1
100	6.6×10^1

Figure 7. Ratio of E'/B' as a function of frequency. There is not an $f^{-1/2}$ dependence throughout the interval. It is speculated that the waves may be propagating off-axis to B_o.

electromagnetic waves at frequencies above the proton cyclotron frequency, but below the electron cyclotron frequency, only the whistler mode (right-hand polarized) exists. At low frequencies, V_{ph} is $\sim V_A$, the Alfvén velocity. At higher frequencies, n will decrease with a $f^{-1/2}$ dependence. From measured values of B_o (5 nT) and ρ (= 0.1 cm^{-3}),we find $V_A = 2.4 \times 10^7$ cm s^{-1} and $n \cong$ 870. This higher value of c/V_A may indicate that the waves are propagating not parallel to the field, but obliquely.

The measured value of B'/E' is reasonably close to the theoretical value, given the errors in the measurements of B' and E'. There is a $f^{-1/2}$ dependence for the frequency range 10^0-10^1 Hz. However, for the 10^1- to 10^2-Hz range, the B'/E' ratio has a positive slope. Since clear E' wave signals were not detected at frequencies above the electron cyclotron frequency (140 Hz), the possibility that these BL waves might be purely electromagnetic remains (however, it should be noted that because of the steep spectrum of the waves, the cutoff might be due more to instrument sensitivity limitations rather than to an actual cutoff of E' signals). We should also mention that *Rezeau et al.* [1989] and *Belmont et al.* [1995] have interpreted these fluctuations at Earth as convected low-frequency Alfvén waves. Our results are not inconsistent with this picture. However, for the wave-particle interaction portion of the paper we will assume the former interpretation and will make conclusions based on this assumption.

A comparison of Jovian waves and the Earth's BL waves is given in Table 2. For the waves at the Earth we use the published results of: a) *Gurnett et al.* 1979], b) *Tsurutani et al.* [1981], c) *Anderson et al.* [1982], d) *Rezeau et al.* [1989] and e) *Tsurutani et al.* [1989] (a,b,c, etc. are indicated in the first column of the table). Although the wave power at Jupiter is lower by several orders of magnitude, we note several similarities of the waves for the two different magnetospheres. Both have power law type spectra without any obvious spectral peaks. The slopes of the electric field spectra are quite similar. Although the terrestrial magnetic field component spectral slope is highly variable depending on the study, the Jovian measurements are within the range of the terrestrial spectral shapes.

Boundary Layer Formation and Thickness

The boundary layer thickness due to cross-field diffusion of magnetosheath plasma can be calculated by assuming resonant wave-particle interactions [*Eviatar and Wolf*, 1968; *Tsurutani and Thorne*, 1982], using the measured wave-particle interactions discussed previously. This same diffusion process will allow the escape of energetic magnetospheric ions into the magnetosheath and into interplanetary space as well.

The cross-field scattering rate is

$$D_{\perp B} \cong 2 (B'/B_o)^2 D_{max} \quad (1)$$

where B_o is the ambient magnetic field and D_{max} is the maximum

Table 2. A comparison of the Jovian BL plasma wave spectra and the Earth's wave spectra

Spacecraft	Location	Date	B'	E'
ISEE 1[a]	Earth magnetopause	day 314, 1977	$\sim f^{-3.3}$	$\sim f^{-2.2}$
ISEE 1 and 2[b]	Earth magnetopause	1977	$(1 \times 10^1) f^{-3.9}$	$(3 \times 10^{-5}) f^{-2.8}$
ISEE 1 and 2[c]	Earth magnetopause	1977	$(7.9 \times 10^{-2}) f^{-2.9}$	$(6.3 \times 10^{-6}) f^{-2.2}$
GEOS 2[d]	Earth magnetopause	day 240, 1978	X: $(3.6 \times 10^1) f^{-2.6}$ Y: $(1.8 \times 10^1) f^{-2.4}$ Z: $(2.8 \times 10^1) f^{-2.7}$	$(1.2 \times 10^{-6}) f^{-2.6}$
ISEE 1[e]	Earth magnetopause	1977-79	$(3 \times 10^{-1}) f^{-3.3}$	$(6 \times 10^{-7}) f^{-2.1}$
Ulysses	Jupiter magnetopause	day 043, 1992	$(2 \times 10^{-4}) f^{-2.4}$	$(4 \times 10^{-9}) f^{-2.4}$

or Bohm diffusion rate. D_{max} is given by

$$D_{max} = E_{\perp} c /2eB_o = 5 \times 10^5 E_{\perp}(\text{keV})/B(\text{nT}) \text{ km}^2 \text{ s}^{-1} \quad (2)$$

where $E_{\perp}$ is the perpendicular kinetic energy of the particle. At the Jovian boundary layer, $B_o \approx 5$ nT. Assuming a magnetosheath proton kinetic energy of 1 keV, D_{max} is 10^5 km^2 s^{-1}. Using a magnetic wave power of $B'^2 \approx 10^{-1}$ nT^2, we get $D_{\perp B'} \approx 10^3$ km^2 s^{-1}. For the timescale of cross-field diffusion we use the convection of magnetosheath plasma from the magnetopause nose to the dawn/dusk flank. A sheath flow velocity of 100 km s^{-1} and a distance of 150 R_J are assumed. We find the BL thickness is predicted to be 10,700 km or ~0.15 R_J thick. From analyses of a Pioneer 10 triple crossing of the magnetopause/plasma boundary layer, *Sonnerup et al.* [1981] determined a thickness of 9100 to 13,000 km. This measurement is in excellent agreement with the above theoretical expectations.

Although the exact correspondence between the boundary layer thickness and the corresponding latitudinal widths at ionospheric heights is difficult to determine, a contraction factor of the magnetic fields of ~60 (L ~ 60) is a reasonable estimate. This would give a ~180 km (150-200 km) latitudinal width at ionospheric/atmospheric altitudes.

Particle Pitch Angle Diffusion

The effects of both the E' component and the B' component of the waves should be analyzed and discussed in terms of effectiveness for pitch angle scattering rates. We use the expressions

$$D^{\pm}_{\alpha\alpha} \sim (B'/B_o)^2 2\pi f_g^{\pm} \eta \quad (3)$$

$$D^{\pm}_{\alpha\alpha} \sim (c/V)^2 (E'/B_o)^2 f_g^{\pm} \eta \quad (4)$$

taken from *Kennel and Petschek* [1966]. In the above expressions, $D_{\alpha\alpha}$ is the diffusion rate due to resonance with the magnetic component of waves (3) and with the electric component (4), respectively. f_g is the particle gyrofrequency, the superscripts + and − are used for protons and electrons respectively, η is the fractional amount of time that the particle is in resonance with the waves, and V is the particle velocity. From measurements we determine $f_g^- \approx 140$ Hz and $f_g^+ \approx 7.6 \times 10^{-2}$ Hz.

Electron Diffusion

To determine B' at cyclotron resonance, we assume first-order resonance:

$$\omega - \vec{k} \cdot \vec{V} = \Omega^{\pm} \quad (5)$$

where $\Omega^{\pm} = 2\pi f_g^{\pm}$. Assuming that the waves are whistler mode (right-hand polarized), the electrons will interact via the ordinary Doppler-shifted resonance condition,

$$\omega + k_{\parallel} V_{\parallel} = \Omega^- \quad (6)$$

giving

$$\omega = (eB/m^- c)/(1 + V_{\parallel}/V_{ph}) \quad (7)$$

Using representative energies of 1-keV to 10-keV for the electrons, we have calculated the resonant frequencies assuming parallel propagating particles. These values, the electromagnetic wave power, diffusion rates, and pitch angle scattering rates are given in Table 3. The pitch angle scattering times are given as $T_{\alpha\alpha}$. Assuming a (conservative) field line at L = 60, the particle bounce times are calculated. By comparing $T_{\alpha\alpha}$ to T_{bounce}, we determine whether the particles are on strong or weak pitch angle diffusion.

The 1-keV electrons are found to be on strong diffusion, while the 10-keV electrons are on near-strong to weak diffusion. Higher-energy electrons are on weak diffusion. Thus, only the 1- to 5-keV electrons need to be considered in the auroral energy calculations.

Proton Diffusion

The protons are a different story. Assuming that the electromagnetic waves at frequencies above the proton cyclotron frequency are whistler mode, then the interaction of protons or ions with these waves will be through an anomalous Doppler-shifted cyclotron resonance where the particles overtake the waves. The first-order resonance can be expressed as

$$\omega - k_{\parallel} V_{\parallel} = -\Omega^+ \quad (8)$$

giving

$$\omega = (eB/m^+ c)/(V_{\parallel}/V_{ph} - 1) \quad (9)$$

Table 3. Diffusion and bounce times for low-energy electrons and protons

Species	f_{res}	Wave Power	$D_{\alpha\alpha}$	$T_{\alpha\alpha}$	T_{bounce}
		Whistler Mode Waves: $D^{\pm}_{\alpha\alpha} = (B'/B_0)^2 2\pi f_g^{\pm} \eta$			
1 keV e^-	2.5 Hz	4×10^{-5} nT^2 Hz^{-1}	9.6×10^{-4}	1.0×10^3 s	1.4×10^3 s
10 keV e^-	0.8 Hz	4×10^{-4} nT^2 Hz^{-1}	1.2×10^{-4}	8.3×10^3 s	4.5×10^2 s
1 keV p^+	2.7×10^{-1} Hz	6×10^{-3} nT^2 Hz^{-1}	1.4×10^{-5}	6.9×10^4 s	6.1×10^4 s
10 keV p^+	2.5×10^{-2} Hz	5×10^{-1} nT^2 Hz^{-1}	1.3×10^{-3}	3.3×10^2 s	1.9×10^4 s
		Electric Waves: $D^{\pm}_{\alpha\alpha} \approx (c/V)^2 (E'/B_0)^2 f_g^{\pm} \eta$			
1 keV p^+	3×10^{-2} Hz	10^{-5} V^2 m^{-2} Hz^{-1}	1.2×10^{-3}	8.2×10^2 s	6.1×10^4 s

From left to right, columns are particle species, resonant frequencies, wave power at the resonant frequencies, pitch angle diffusion rates, pitch angle scattering timescales, and bounce periods (assuming L=60 magnetic field lines).

Calculations similar to those done for resonant electrons are given in Table 3. The 1- to 10-keV protons are on near-strong diffusion, and the >10-keV energy protons are on strong diffusion. The diffusion rate is higher for more energetic particles. The higher the particle energy, the lower the resonant frequency. Because the waves have a power law dependence, the higher wave power at lower frequencies leads to greater diffusion rates. For calculation purposes we consider protons up to 1-MeV energies. These particles will be on strong diffusion.

We have also examined the proton pitch angle diffusion rates due to cyclotron resonance with electric waves. We find the diffusion rates for 1-keV protons are quite rapid and these particles are on strong diffusion due to this interaction.

From the analyses of the pitch angle diffusion rates due to both the magnetic component and the electric component of the waves, 1- to 5-keV electrons and 1-keV to 1-MeV protons are on strong diffusion. Lower-energy, <1-keV plasma will also be on strong diffusion. We have also assumed that the ions are protons. If they are in actuality heavier ions (He^{++}, oxygen, or sulfur), the energy flux will be less (these numbers have been calculated but are not shown so as to conserve space).

Particle Precipitation Rates

Figure 8 shows two energetic electron spectra. The count rates from two detector heads (pitch angles) are given in the figure. The count rates (circles) are nearly the same, indicating that the pitch angle distribution is nearly isotropic. Our calculations show that the 1- to 5-keV energy range (outside the instrument range) should be on strong diffusion, but they do not explain this phenomenon at higher energies.

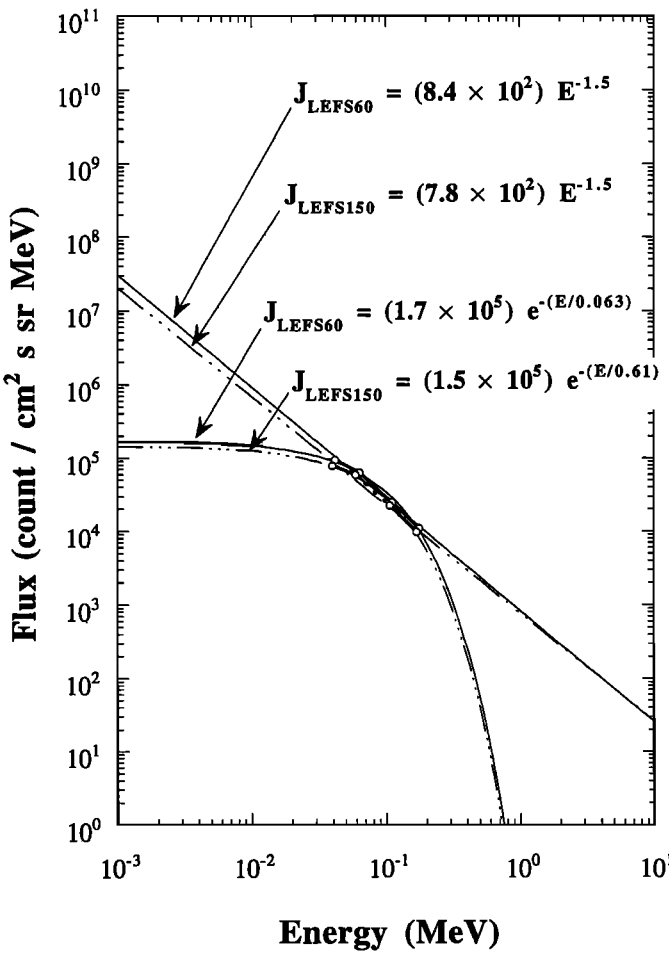

Figure 8. Energetic electron spectra for event 10.

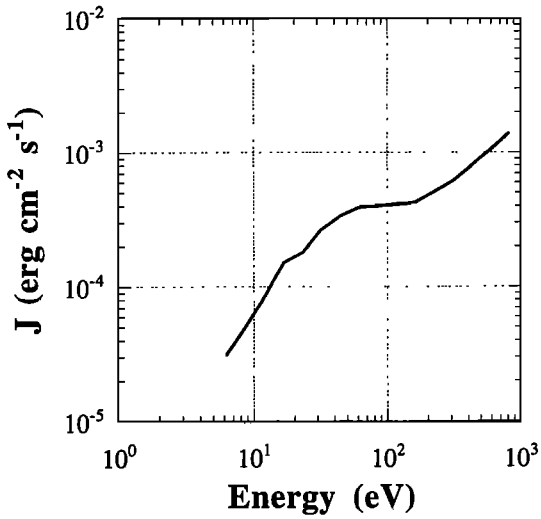

Figure 9. The <1 keV electron spectrum for event 10.

Power law and exponential fits to the electrons are shown in Figure 8. The former is an upper limit, while the latter is a conservative approximation. We will use the former fit to estimate the upper boundary of auroral energy flux from 1- to 5-keV.

The low-energy electron spectrum from the solar wind plasma experiment [*Bame et al.* 1992b] is given in Figure 9. The energy range is 6-eV to 815-eV. The total integrated energy is 0.006 erg cm^{-2} s^{-1}. It should be noted that the energy flux is increasing with energy and the peak had not been reached by 815 eV. Clearly, the peak lies somewhere between the plasma instrument and HI-SCALE energy thresholds.

The energetic proton spectrum is given in Figure 10. The protons are fitted by a power law approximation. This seems to be a better fit than an exponential one. It should be reasonably accurate in the 10- to 100-keV range but may be on the high side for 1- to 10-keV energies.

The energy deposition rate as a function of species and energy ranges has been calculated. We find that the total energy of precipitating ions from 1-keV to 1-MeV is 0.11 erg cm^{-2} s^{-1}, and for electrons in the same energy range it is 0.02 erg cm^{-2} s^{-1}, giving a total energy flux of 0.13 erg cm^{-2} s^{-1}.

Imaging Observations

Energetic particles that have been pitch angle scattered into the atmospheric loss cone follow the magnetic field lines down to the ionosphere/atmosphere of Jupiter, where they give rise to collisionally excited auroral emissions. For the major species in the Jovian atmosphere, atomic and molecular hydrogen, the resulting electronic transitions lie in the far ultraviolet (FUV) wavelength range.

The first HST images of the Jovian aurorae were taken during the flyby of Ulysses, on February 7 and 9, 1992, with the faint object camera (FOC). For these observations the combination of the HST spherical aberration and nonoptimal choices of wavelength ranges resulted in a moderate spatial resolution only (~0.2-0.5 arc sec; i.e., 700-1800 km projected on the planetary disc). However, the basic morphology of the auroral emission derived from these observations was confirmed by the following HST observations, which took place regularly at least twice a year until the present [*Gérard et al.*, 1993; *Clarke et al.*, 1995],

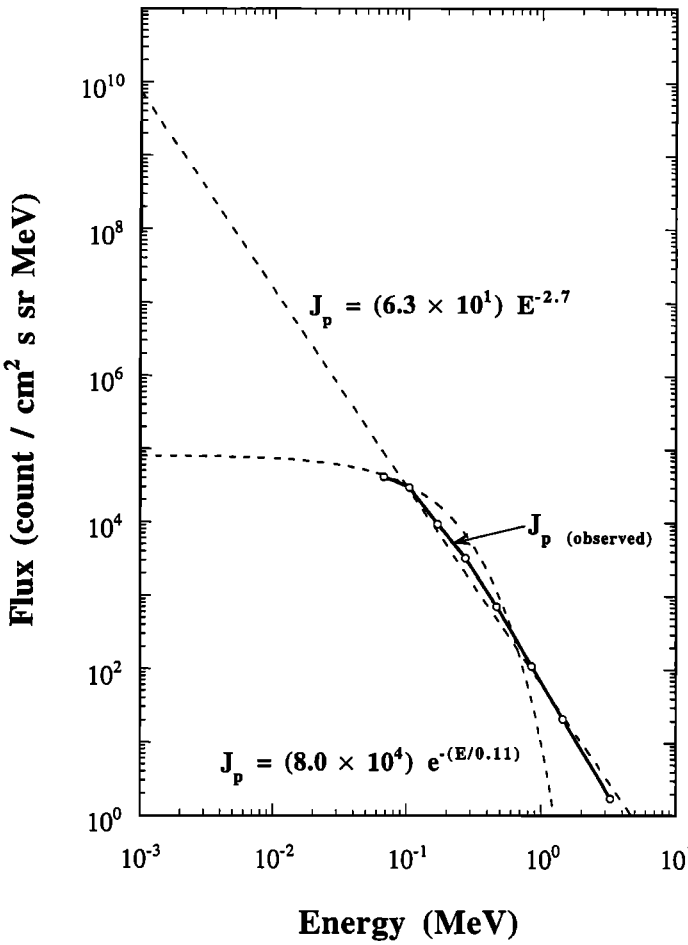

Figure 10. Energetic ion (protons) spectra for event 10.

including the last set of data obtained in July-August 1994 where the FOC had a much better spatial resolution after correction for telescope aberration [*Prangé et al.*, 1996b]. The brightest feature identified in the images is a very narrow oval that surrounds each pole at high latitudes. The oval looks amazingly narrow, regular, and continuous along tens of thousands of kilometers, although some very localized discrete emissions are superimposed (it looks much more regular than the discrete auroral emission on the Earth's nightside). This finding suggests that the precipitating particles map into a well-defined and stable large-scale layer in the outer magnetosphere. This oval is in general relatively close to the footprint of magnetic field lines crossing the equatorial plane near 30 R_J. However, this determination is not quite accurate. Present models cannot precisely account for the high-order terms of the magnetic potential close to Jupiter's surface, and recent new constraints on the surface magnetic field, imposed by the trace of Io's magnetic footprint, suggest that it could be on higher latitude field lines. In the case of the February 1992 images, where the magnetosphere was particularly inflated, correlations with simultaneous Ulysses particles and field measurements, taken at 20 R_J from the planet, have shown that the emissions were likely to originate from the footprint of magnetic field lines just equatorward of the polar cap boundary, which crossed the equatorial plane near about 40-60 R_J [*Prangé et al.*, 1993, *Dougherty et al.*, 1996]. In addition to this bright oval, a series of fainter concentric ovals, very narrow as well, have also been observed at higher latitude. Whether these faint ovals are on open or closed field lines is not known.

Several factors may limit our ability to determine the intrinsic width of a narrow feature. The most important ones are the overall spatial resolution of the instrument and the smearing of the feature due to the rotation of the planet during the exposures. The images obtained in 1994 provide for the first time very good conditions for an estimate of the latitudinal extent of the high-latitude oval. The pixel size used is now 0.014 × 0.028 arc sec^2. The point spread function (PSF) encircles 50% of the energy at this wavelength within a radius of <0.05 arc sec, and for one-dimensional sources the transverse resolution reaches ≅0.035 arc sec, i.e., ≅ 120-150 km on the planetary disc, depending on the distance of the planet (exceeding by far the capabilities of any past or existing instrument). In order to minimize the effect of the smearing during the 11- to 12- min exposures (about 7°) we use the southern oval (more symmetric than the northern one, see Figure 3 of *Clarke et al.*, [1995] and Figure 1 of *Prangé et al.*, [1996b], and along this oval we select regions where the oval is most nearly aligned at constant latitude (so that rotating point sources follow the oval locus).

Figure 11a shows a plot across the high-latitude oval, integrated over 50 pixels along the oval. We have selected here the narrowest auroral segment from our high spatial resolution images. The background disc emission has been derived from another image where the oval is mainly hidden on the nightside. The excess emission, which consists of a peak surrounded by some diffuse emission on both sides, is due to auroral excitation. The peak is extremely narrow, 2.2 pixels full width at half maximum, or 0.062 arc sec (Figure 11b). By taking into account the instrument spatial resolution the resulting intrinsic width of the auroral emission drops to about 0.05 arc sec, corresponding to a 180-km auroral structure projected on the disc. Visual inspection of the oval suggests a very small bending of the oval resulting in a broadening of the order of 0.1-0.2° latitude, or about 50-100 km on the disc. Projected perpendicular to the magnetic field lines at the latitude of the emission, this produces a sheet about 230 ±100 km wide. This incredibly small value is still an upper limit, because it includes the additional broadening due to any small-scale curvature of the oval along the 5000 km of the cut, as well as some remaining noise in the data. The peak intensity corresponds to a brightness of ≅475 ± 50 kR. By using a model of particle energy degradation in the atmosphere [*Rego et al.*, 1994], the energy conversion factor has been estimated for a wide range of incident particles, 1-keV to 200-keV electrons and 25-keV to 1-MeV protons [D. Rego, private communication, 1996]. The peak energy input flux from the magnetosphere in this segment of arc is thus estimated to range between 20 and 50 ergs cm^{-2} s^{-1}. Plots across different parts of the oval or at different dates show that the width of the arc may extend up to about 500 km, with peak energy deposition values up to 150 ergs cm^{-2} s^{-1}. However, one must note that there is some indication of multiple sheet-fine structure in the broader features, although they cannot be properly resolved at the FOC resolution.

The present identification of such a narrow region of intense precipitation defines a very specific magnetospheric layer as the origin of the particle losses. The narrowness of this region, together with the very high latitude field lines concerned (close to the polar cap boundary), had initially led to the suggestion that the precipitation could be triggered by field-aligned currents [*Prangé et al.*, 1993; *Gérard et al*, 1994]. Generation of the BL plasma waves by such currents is consistent with all of the observations.

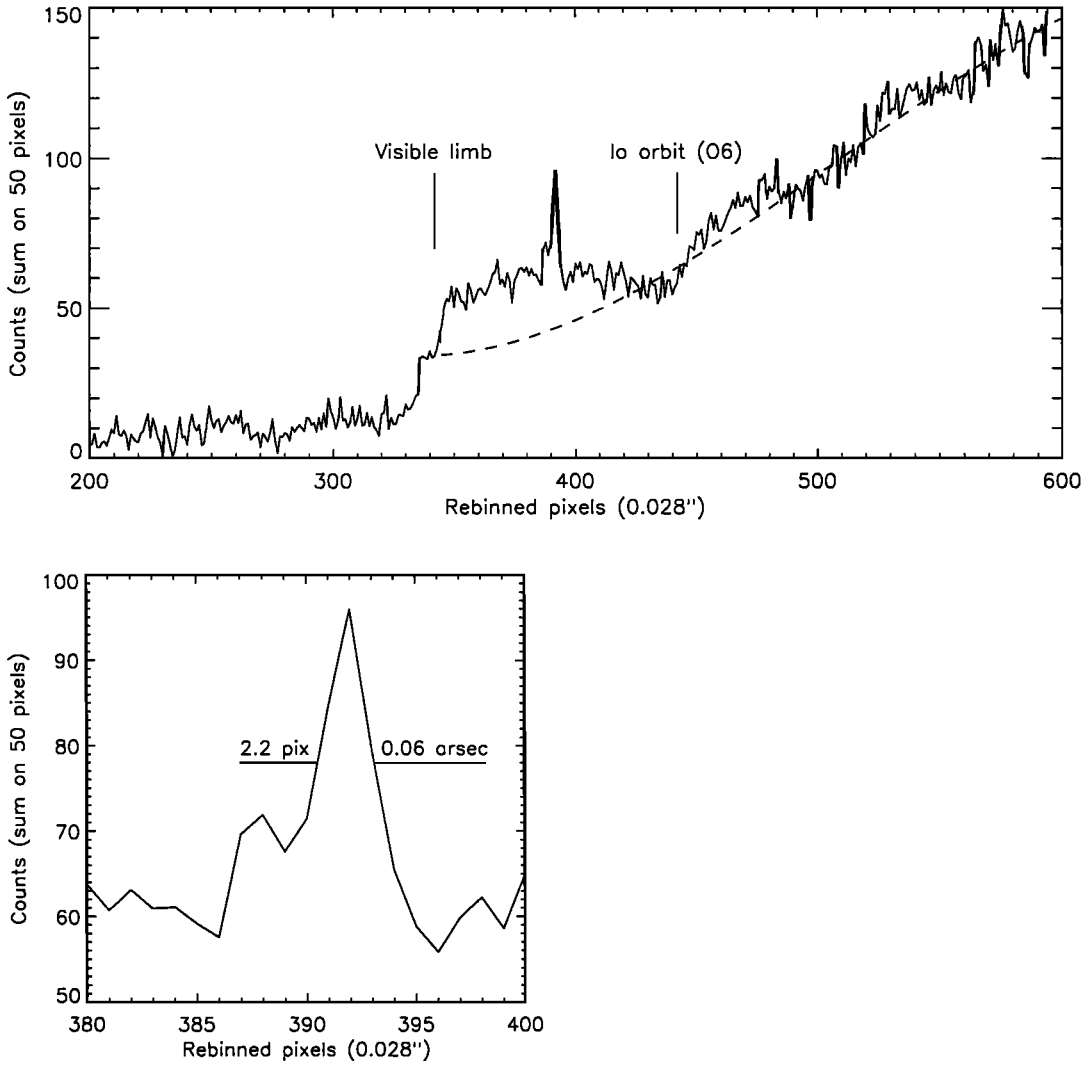

Figure 11. (a) Plot across the southern hemisphere of the Jupiter auroral oval on an image taken with the Faint object camera aboard HST on July 13, 1994. The filters used isolate the collisionally excited H_2 Lyman bands around 1550 Å. The counts are integrated along a north-south strip 50 pixels wide (~5000 km). The dashed line is a fit across another image at the same wavelength, but when the other side of the planet is facing the Earth. It is used as a reference of the solar scattered flux from the planetary disc. One can note a region between the limb and the magnetic footprint of the orbit of Io, where there is an excess of emission from the aurorae. Near the center of the auroral emission area one can see the narrow bright auroral oval. (b) Magnified plot across the auroral oval with the background emission removed. Abscissa are pixel numbers toward the equator, and ordinates are total counts.

Summary and Conclusions

1. It has been shown that the Jovian BL plasma waves have sufficient intensity to cause cross-field diffusion of magnetosheath plasma across the magnetopause to create the BL itself [*Tsurutani et al.*, 1993]. The predicted thickness is in agreement with in situ measurements [*Sonnerup et al.*, 1981].

2. A comparison of the Jovian BL plasma wave spectra and the Earth's BL plasma wave spectra (Table 2) has shown that the waves are quite similar. The electric field spectral shape is similar to the terrestrial counterpart. The terrestrial wave magnetic field component is highly variable, depending on the study. However, the Ulysses wave magnetic field component spectral shapes are within the range of shapes reported from the terrestrial wave studies.

3. It should be noted that the Jovian BL wave amplitudes are considerably smaller than those at the Earth. In general, they are orders of magnitude smaller (Table 2). This finding should be noted for future missions to Jupiter (or Saturn). Experiments designed to measure such waves will need be even more sensitive than the URAP instrument (which is already greatly improved over past deep space missions).

4. The Jovian time-averaged wave spectra are more or less smooth power laws, to first order. There are no obvious spectral features that would indicate a particular plasma instability for a generation mechanism. This case is similar to that for the Earth's BL waves. However, we are currently examining the ELF/VLF wave data in greater detail to see whether or not subtle wave structure is present.

5. The Jovian BL waves have been detected at approximately noon and also at approximately dusk, two different local time regions. The waves may therefore be present at all locations on the dayside magnetopause. If this is the case, the situation would be the same as that for the Earth's BL waves [*Tsurutani et al.* 1989].

6. The ratio of B'/E' does not have a $f^{-1/2}$ dependence throughout the range of measurements. This finding may indicate that the waves are obliquely propagating in the whistler mode.

7. The Jovian BL wave intensities appear to be dependent on the external solar wind ram pressure. The waves are an order of magnitude more intense on the outbound leg, where the ram pressure was more typical (the ram pressure during the inbound leg was anomalously low). This finding is different from that of *Tsurutani et al.* [1989] that the terrestrial BL wave intensities were independent of magnetosheath |B|.

8. The width of the Jovian BL mapped down to the ionosphere is ~150-200 km. The location of the BL waves will be on field lines at and inside the last closed field line.

9. It has recently been discovered from Polar satellite plasma wave observations [*Ho et al.*, 1996] that the Earth's boundary layer waves encompass all local times, including nightside auroral regions. Thus the most likely source of the broadband waves is field-aligned currents or current gradients. Although a complete survey for the Jovian magnetosphere has not been completed (by Galileo), our Ulysses survey indicates a similar BL wave local time dependence at Jupiter.

10. Calculations indicate that 1- to 5-keV (and lower) electrons and 1- to 1,000-keV protons (and lower) are on strong pitch angle diffusion. The total energy of 1-keV to 1-MeV electrons and protons is 0.02 erg cm^{-2} s^{-1}, and 0.11 erg cm^{-2} s^{-1}, respectively. This precipitation energy flux into the Jovian polar ionosphere will cause a weak auroral ring.

11. The intense Jovian aurora is dominated by continuous rings centered about the poles. These "main ovals" can be as narrow as 230 ± 100 km in width. We note that the Jovian BL has the same width at ionospheric heights and if the BL exists everywhere along the Jovian magnetopause, the BL will also map into high latitude rings centered about the poles. If it is found that the presence of higher order moments of the Jovian intrinsic magnetic field and the presence of the extended magnetospheric current sheet/disc leads to a reinterpretation that the aurora occurs on BL magnetic field lines, then we have shown that magnetospheric wave-particle interactions are not directly responsible for such auroral intensities. Ionospheric processes (such as acceleration within double layers) must be dominant.

Acknowledgments: Portions of this research effort were performed at the Jet Propulsion Laboratory, California Institute of Technology, Pasadena, under contract with the National Aeronautics and Space Administration. Part of the search coil data analyses was supported by CNES, the French Space Agency. We are indebted to D. Rego for calculations of the auroral energy conversion factor. R. Prangé was supported by the Centre National de La Recherché Scientifique and by grants from the Programme National de Planetologie of the Institut National des Sciences de l'Univers and CNRS-GdR Plasmae.

The Editor thanks R. M. Thorne and G. R. Gladstone for their assistance in evaluating this paper.

References

Anderson, R. R., C. C. Harvey, M. M. Hoppe, B. T. Tsurutani, T. E. Eastman, and J. Etcheto, Plasma waves near the magnetopause, *J. Geophys. Res.*, *87*, 2087, 1982.

Ashour-Abdalla, M., and R. M. Thorne, The importance of the electrostatic ion-cyclotron instability for quiet-time proton auroral precipitation, *Geophys. Res. Lett.*, *4*, 45, 1977.

Axford, W. I., and C. O. Hines, A unifying theory of high-latitude geophysical phenomena and geomagnetic storms, *Can. J. Phys.*, *39*, 1433, 1961.

Balogh, A., T. J. Beek, R. J. Forsythe, P. C. Hedgecock, R. J. Marquedant, E. J. Smith, D. J. Southwood, and B. T. Tsurutani, The magnetic field investigation on the Ulysses mission: Instrumentation and preliminary scientific results, *Astron. Astrophys. Suppl. Ser.*, *92*, 221, 1992.

Bame, S. J., B. L. Barraclough, W. D. Feldman, G. R. Gisler, J. T. Gosling, D. J. McComas, J. L. Phillips, and M. F. Thomsen, Jupiter's magnetosphere: Plasma description from the Ulysses flyby, *Science*, *257*, 1539, 1992a.

Bame, S. J. D. J. McComas, B. L. Barraclough, J. L. Phillips, K. J. Sofaly, J. C. Chavez, B. E. Goldstein, and R. K. Sakurai, The Ulysses solar wind plasma experiment, *Astron. Astrophys. Suppl. Ser.*, *92*, 237, 1992b.

Belmont, G., F. Reberac, and L. Rezeau, Resonant amplification of magnetosheath MHD fluctuations at the magnetopause, *Geophys. Res. Lett.*, *22*, 295, 1995.

Clarke, J. T., et al., HST far-ultraviolet imaging of Jupiter during the impacts of comet Shoemaker-Levy 9, *Science*, *267*, 1302, 1995.

Cole, K. D., On the solar wind generation of polar geomagnetic disturbance, *Geophys. J. R. Astron. Soc.*, *6*, 103, 1961.

D'Angelo, N., Ultralow-frequency fluctuation at the polar cusp boundaries, *J. Geophys. Res.*, *78*, 1206, 1973.

Dougherty, M. K., M. Dunlop, and R. Prangé, Identification of a current-driven auroral on Jupiter with correlated Ulysses and HST observations, *Planet. Space Sci.*, in press, 1996.

Drake, J. F., J. Gerber, and R. G. Kleva, Turbulence and transportation in the magnetopause current layer, *J. Geophys. Res.*, *99*, 11,211, 1994.

Eviatar, A., and R. W. Wolf, Transfer processes in the magnetosphere, *J. Geophys. Res.*, *73*, 5561, 1968.

Galvin, A. B., C. M. S. Cohen, F. M. Ipavich, R. von Steiger, J. Wock, and U. Mall, Boundary layer ion composition at Jupiter during the inbound pass of the Ulysses flyby, *Planet. Space Sci.*, *41*, 869, 1993.

Gehrels, N., and E. C. Stone, Energetic oxygen and sulphur ions in the Jovian magnetosphere and their contributions to the auroral excitation, *J. Geophys. Res.*, *88*, 5537, 1983.

Gendrin, R., Magnetic turbulence and diffusion processes in the magnetopause boundary layer, *Geophys. Res. Lett.*, *10*, 769, 1983.

Gérard, J.-C., V. Dols, F. Paresce, and R. Prangé, Morphology and time variation of the Jovian far UV aurora: Hubble space telescope observations, *J. Geophys. Res.*, *98*, 18,793, 1993.

Gérard, J. C., V. Dols, R. Prangé, and F. Paresce, The morphology of the north Jovian ultraviolet aurora observed with the Hubble space telescope, *Planet. Space Sci.*, *42*, 905, 1994.

Gurnett, D. A., R. R. Anderson, B. T. Tsurutani, E. J. Smith, G. Paschmann, G. Haerendel, S. J. Bame, and C. T. Russell, Plasma wave instabilities at the magnetopause: Observations from ISEE 1 and 2, *J. Geophys. Res.*, *84*, 7043, 1979.

Herbert, F., B. R. Sandel, and A. L. Broadfoot, Observations of the Jovian UV aurora by Voyager, *J. Geophys. Res.*, *92*, 3141, 1987.

Ho, C. M., B. T. Tsurutani, J. K. Arballo, A. Boonsiriseth, D. M. Mueller, R. R. Anderson, D. A. Gurnett, G. K. Parks, and R. M. Thorne, Plasma waves in the magnetopause boundary layer and the dayside aurora: Polar observations, paper presented at SOLTIP III, organized by SOLTIP, cosponsored by SCOSTEP and the Chinese Academy of Sciences, Beijing, China, Oct. 1996.

Huba, J. D., N. T. Gladd, and K. Papadopoulos, Lower-hybrid-drift wave turbulence in the distant magnetotail, *J. Geophys. Res.*, *83*, 5217, 1978.

Kennel, C. F., and H. E. Petschek, Limit on stably trapped particle fluxes, *J. Geophys. Res.*, *71*, 1, 1966.

LaBelle, J., and R. A. Treumann, Plasma waves at the dayside magnetopause, *Space Sci. Rev.*, *47*, 175, 1988.

Lanzerotti, L. J., S. M. Krimigis, C. O. Bostrom, W. I. Axford, R. P. Lepping, and N. F. Ness, Measurements of plasma flow at the dawn magnetopause by Voyager 1, *J. Geophys. Res.*, *84*, 6483, 1979.

Lanzerotti, L. J., et al., Heliospheric instrument for spectra, composition and anisotropy at low energies, *Astron. Astrophys. Suppl. Ser.*, *92*, 349, 1992.

Phillips, J. L., S. J. Bame, M. F. Thomsen, B. E. Goldstein, and E. J. Smith, Ulysses plasma observations in the Jovian magnetosheath, *J. Geophys. Res.*, *98*, 21,189, 1993.

Prangé, R., and M. Elkhamsi, Modeling the precipitation flux in the Jovian auroral zones, 1 The model and its application to the UV auroral emissions of Jupiter, *J. Geophys. Res.*, *96*, 21,371, 1991.

Prangé, R., N. Dougherty, and V. Dols, Identification d'une aurorae "current-driven" sur Jupiter, á l'aide d'observations corrélées avec HST et Ulysses, in *Compte-rendus du Séminaire scientifique du GdR Plasmae*, edited by D. Hubert, DESPA-Observatoire de Paris, 38, 1993.

Prangé, R., D. Rego, D. Southwood, P. Zarka, S. Miller, and W. Ip, Rapid energy dissipation and variability of the Io-Jupiter electrodynamic circuit, *Nature*, *379*, 323, 1996a.

Prangé, R., S. Maurice, W. M. Harris, D. Rego, and T. Livengood, Comparison of IUE and HST diagnostic of the Jovian aurorae, *J. Geophys. Res.*, in press, 1996b.

Rego, D., R. Prangé, and J.-C. Gérard, Auroral Lyman α and H_2 bands from the giant planets, 1, Excitation by proton precipitation in the Jovian atmosphere, *J. Geophys. Res.*, *99*, 17,075, 1994.

Rezeau, L., A. Morane, S. Perraut, A. Roux, and R. Schmidt, Characterization of Alfvénic fluctuations in the magnetopause boundary layer, *J. Geophys. Res.*, *94*, 101, 1989.

Rezeau, L., N. Cornilleau-Wehrlin, G. Belmont, P. Canu, R. Prangé, A. Balogh and R. J. Forsythe, Possible role of electromagnetic low frequency waves in the Io torus in the production of Jovian aurorae, in press, *Planet. Space Sci.*,1996.

Scudder, J. D., E. C. Sittler, and H. S. Bridge, A survey of the plasma electron environment of Jupiter: A view from Voyager, *J. Geophys. Res., 86*, 8157, 1981.

Smith, E. J., and K.-P. Wenzel, Introduction to the Ulysses encounter with Jupiter, *J. Geophys. Res., 98*, 21,111, 1993.

Sonnerup, B.U.O., E. J. Smith, B. T. Tsurutani, and J. H. Wolfe, Structure of Jupiter's magnetosphere: Pioneer 10 and 11 observations, *J. Geophys. Res., 86*, 3321, 1981.

Stone, R. G. et al., The unified radio and plasma wave investigations, *Astron. Astrophys. Suppl. Ser., 92*, 291, 1992.

Swift, D., Turbulent generation of electrostatic fields in the magnetosphere, *J. Geophys. Res., 82*, 5143, 1977.

Thorne, R. M., Jovian auroral secondary electrons and their influence on the Io plasma torus, *Geophys. Res. Lett., 8*, 509, 1981.

Thorne, R. M., Microscopic plasma processes in the Jovian magnetosphere, in Physics of the Jovian Magnetosphere, edited by A. J. Dessler, 454, Cambridge University Press, New York, 1983.

Thorne, R. M., and J. Moses, Electromagnetic ion-cyclotron instability in the multi-ion Jovian magnetosheath, *Geophys. Res., Lett., 10*, 631, 1983.

Thorne, R. M., and B. T. Tsurutani, Diffuse Jovian aurora influenced by plasma injection from Io, *Geophys. Res. Lett., 6*, 649, 1979.

Thorne, R. M., and B. T. Tsurutani, Wave particle interactions in the magnetopause boundary layer, in *Physics of Space Plasmas (1990)*, 10, edited by T. Chang et al., p. 119, Sci. Publ., Cambridge, Mass., 1991.

Tsurutani, B. T., and W. D. Gonzalez, The efficiency of "viscous interaction' between the solar wind and the magnetosphere during intense northward IMF events, *Geophys. Res. Lett., 22*, 663, 1995.

Tsurutani, B. T., and R. M. Thorne, Diffusion processes in the magnetopause boundary layer, *Geophys. Res. Lett., 9*, 1247, 1982.

Tsurutani, B. T., E. J. Smith, R. M. Thorne, R. R. Anderson, D. A. Gurnett, G. K. Parks, C. S. Lin, and C. T. Russell, Wave-particle interactions at the magnetopause: Contributions to the dayside aurora, *Geophys. Res. Lett., 8*, 183, 1981.

Tsurutani, B. T., A. L. Brinca, E. J. Smith, R. T. Okida, R. R. Anderson, and T. E. Eastman, A statistical study of ELF-VLF plasma waves at the magnetopause, *J. Geophys. Res., 94*, 1270, 1989.

Tsurutani, B. T., D. J. Southwood, E. J. Smith, and A. Balogh, A survey of low-frequency waves at Jupiter:. The Ulysses encounter, *J. Geophys. Res., 98*, 21,203, 1993.

B. T. Tsurutani and E. J. Smith, J. K. Arballo, B. E. Goldstein, C. M. Ho, G. S. Lakhina, Jet Propulsion Laboratory, California Institute of Technology, 4800 Oak Grove Drive, Pasadena, California 91109. (email: btsurutani@jplsp.jpl.nasa.gov, esmith@jplsp.jpl.nasa.gov, jarballo@jplsp.jpl.nasa.gov, bgoldstein@jplsp.jpl.nasa.gov, cho@jplsp.jpl.nasa.gov, lakhina@jplsp.jpl.nasa.gov).

A. Balogh, Imperial College of Science and Technology, The Blackett Laboratory, Prince Consort Road, London SW7 2BZ, England. (e-mail: abalogh@ic.ac.uk)

N. Cornilleau-Wehrlin, Centre d'Etude des Environnements Terrestre et Planétaires/Université Versailles-Saint-Quentin, 10-12 Avenue de l'Europe, 78140 Vélizy, France. (e-mail: nicole.cornilleau@cetp.ipsl.fr)

M. Kane, Applied Physics Laboratory, Johns Hopkins University, Laurel, MD 20707. (e-mail: mark_kane@jhuapl.edu)

N. Krupp, Max-Planck-Institut für Aeronomie, D-37189, Katlenburg-Lindau, Germany. (e-mail: krupp@camwst.mpae.gwdg.de)

N. Lin and P. Kellogg, University of Minnesota, School of Physics and Astronomy, Minneapolis, MN 55455. (e-mail: waves::kellogg; waves::lin)

J. L. Phillips, Los Alamos National Laboratory, Los Alamos, New Mexico 87544. (e-mail: jlphillips@lanl.gov)

R.Prangé, Institut d'Astrophysique Spatiale, Batiment 121, Université Paris XI, 91405 Orsay Cedex, France. (e-mail: prange@ias.fr)

(Received May 3, 1996; revised September 5, 1996;
accepted September 6, 1996.)